X-ray standing-wave study of $(AlAs)_m(GaAs)_n$ short-period superlattices

A. Lessmann,* S. Brennan, and A. Munkholm†
Stanford Synchrotron Radiation Laboratory SSRL/SLAC, 2575 Sand Hill Road, Menlo Park, California 94025

M. Schuster and H. Riechert
Siemens AG, Corporate Technology, Otto-Hahn-Ring 6, D-81739 Munich, Germany

G. Materlik
Hamburger Synchrotronstrahlungslabor HASYLAB am Deutschen Elektronen-Synchrotron DESY, Notkestrasse 85, D-22603 Hamburg, Germany

(Received 9 April 1998)

X-ray standing-waves (XSW) are used for an investigation of the structure of $(AlAs)_m(GaAs)_n$ short-period superlattices (SL's). The XSW induced modulation of x-ray fluorescence from the Al, As, and Ga atoms and the total photoelectron yield are monitored around the 0th order SL satellite (AlAs)(GaAs)(004,0) and the GaAs(004) substrate Bragg reflection. From the specific shape of these modulations and the sample reflectivity, an atomic model about the interfaces is derived. This is accomplished by comparing the experimental data with dynamical calculations of x-ray wavefield distribution and reflectivity, which are based on the Takagi-Taupin equation. The fluorescence measurements at the 0th order SL satellite reveal a high crystalline order in the AlAs layers of the short-period SL, whereas in the GaAs layers, a fraction of the Ga and As atoms is not on the ideal lattice positions. From the analysis, a model of the atomic distribution along the [001] direction can be determined. This reveals that at each internal interface in the GaAs layers, two Ga atom planes are shifted by up to 0.035 nm and one As atom plane by 0.023 nm. At each interface, the shifts are directed towards the substrate. In addition, the XSW field at the GaAs(004) substrate reflection results in a moiré or beating effect in the SL structure, which can be used to determine the information depth Λ_e of total electron-yield measurements in a more detailed approach. [S0163-1829(99)12715-2]

I. INTRODUCTION

Short-period superlattices (SL's) consisting of very thin alternating AlAs and GaAs layers exhibit certain physical properties, which make them interesting for engineering electronic devices and also for fundamental research. Possible applications are impurity traps with internal gettering at each interface between the two layers, or Bloch oscillators, which utilize the periodically changing electronic structure in the SL. The nearly identical lattice constants of aluminum arsenide and gallium arsenide, as well as advances in molecular beam epitaxy (MBE) technology, made feasible short-period SL's with hundreds of layers and layer thicknesses of only a few monolayers. It is also possible to vary the deposition times during MBE to produce almost any compositional gradient. For a further improvement of the epitaxial perfection at the interfaces, a detailed knowledge of the atomic arrangement, depending on preparation conditions, is important.

A nondestructive method for studying these structural properties is x-ray diffraction, by which the reflectivity $R=|D_H|^2/|D_0|^2$ of a diffracted beam scanning the reciprocal lattice vector $\mathbf{H}$ is monitored. D_0 and D_H are the complex amplitudes of the dielectric displacement of the incident and diffracted x-ray wave. Growth-related parameters such as the superlattice period length d_{SL}, the average concentration ratio of AlAs to GaAs, and the total thickness of the SL can be deduced from the spacing of the SL satellite reflections, the position of the 0th order satellite, and the separation of the thickness fringes.[1] From the satellite intensities, information about fluctuations in the periodicity and interfacial widths can be obtained.[2,3] Harada and co-workers have developed a Fourier method, which is in principle able to give both the concentration and atomic displacement modulation of superlattice structures from the measurement of intensities of satellite reflections.[4] For a structural investigation of the atomic sites of interfaces between the GaAs and AlAs layers, this method depends on the precise measurement of the integral intensities of many satellite reflections and on certain phase assumptions. In short-period SL's this method is limited by the relatively small number of measurable satellite reflections.

If, in addition, the local intensity of the electromagnetic field $|(D_0+D_H)|^2$ at the atomic positions is probed by measuring inelastic secondary processes, the phase of the x-ray wave also becomes accessible. Examples of these signals in x-ray standing-wave (XSW) measurements are the x-ray fluorescence and Auger or photoelectron yields. XSW uses the interference between the incident and reflected x-ray wave, which results in a standing wavefield with an intensity distribution $|(D_0+D_H)|^2$. The nodes and antinodes of this wavefield lie on planes perpendicular to $\mathbf{H}$ with a periodicity given by $2\pi/|\mathbf{H}|$. Commonly used reflections for XSW are Bragg and Laue reflections from single or mosaic crystals (e.g., Refs. 5 and 6), multilayer reflections from synthetic multilayered structures at small incidence angles,[7] and the total reflection near the critical angle.[8] From the comparison of measured XSW induced modulations with theoretical cal-

culations for the field distribution, the atomic positions p_H relative to the wavefield **H** can be extracted. The position $0 \leqslant p_H \leqslant 1$ is given in units of the wavefield periodicity.

Another parameter resulting from the evaluation is the coherent fraction $0 \leqslant f_{c,H} \leqslant 1$, which is, if only one atomic site p_H is occupied, equal to the fraction of atoms located there. The remaining atoms $(1-f_{c,H})$ are uniformly distributed. In general, $f_{c,H}$ is the amplitude $|A_H|$ of the **H** Fourier component $A_H = |A_H| \exp(i\Phi_H)$ of the corresponding periodic atomic-distribution function.[6] The phase of this Fourier component is $\Phi_H = 2\pi p_H$. The contribution to each position p_H (Ref. 9) has to be weighted with the exponential factor $\exp(-z/\Lambda)$, where z is the distance to the surface and Λ the information depth[10] of the signal used. Further details of this data evaluation are described in Sec. II B.

In this paper, the dynamical calculation of depth and incident angle-dependent wavefield in the SL is accomplished by using recursion formulas for a solution of the Takagi-Taupin equation.[11] Theoretical curves were fitted to the data, which were recorded at the 0th order SL satellite (AlAs)(GaAs)(004,0) and the GaAs(004) substrate reflection. In order to probe different depths in the sample, the x-ray fluorescence and the total photoelectron yield were monitored during the XSW measurements. The fluorescence is not as surface sensitive as the electron yield, but has the advantage of being element specific, whereas the nonelement specific total electron yield is averaging over the atomic positions from Al, As, and Ga atoms in a thin surface-region. In general, the information depth[10] of the fluorescence signal Λ_γ and of the photocurrent signal Λ_e can be used to describe the relative contribution to the total signal originating from depth z, which is $\exp(-z/\Lambda_{\gamma,e})$. For the fluorescence, Λ_γ can be calculated from the take-off angle α and the cross section for photoabsorption. In the case of the electron yield, which was measured in a total current mode, a simple evaluation is not possible. However, the XSW results obtained at the GaAs(004) reflection made it feasible to determine Λ_e with otherwise unequalled accuracy.

II. METHOD

A. Experiment

The XSW measurements were performed at beamline 2-2 of the Stanford Synchrotron Radiation Laboratory, where a white beam from a bending magnet is available. After monochromatization and collimation by a symmetric/asymmetric Ge(004) double-crystal monochromator, the size of the beam was limited by slits to illuminate a sample area of 2×2 mm. The photon energy was 5300 eV. The asymmetry parameter of the monochromator was $b = -8$. The Ge(004) monochromator had the advantage that the lattice-plane distance $d_{(004)}(\mathrm{Ge}) = 0.14145$ nm is between that of AlAs and GaAs, resulting in an almost nondispersive arrangement for both substrate reflection and 0th order SL satellite. As a result, the rocking curves were not significantly broadened and the observed phase contrast of the XSW yields were close to the theoretical maximum. For the detection of the total photoelectron yield, the crystals were electrically contacted and placed into small Kapton housings flushed with helium. A ring anode at a potential of 45 V with respect to the sample was placed around the illuminated area to accelerate the emerging photoelectrons.[12] The resulting photocurrent I_e of the order of $10^{-10}A$ was amplified by a current amplifier attached to the sample. Fluorescence photons were recorded by a thin-window solid-state Si(Li) detector[13] aligned in the plane of polarization of the incoming light. At a distance of 15 mm, the average take-off angle between the illuminated spot on the sample surface and the detector crystal was $\alpha = 5°$. The intensities of the incoming as well as the diffracted beam were monitored by ion chambers. Further details of the experimental setup are described in Refs. 3 and 14.

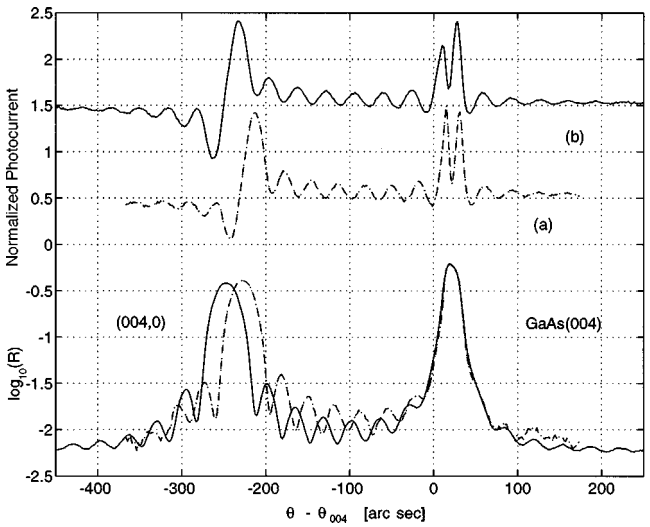

FIG. 1. Logarithm of the reflectivity (bottom part) and linear photocurrent I_e normalized to the off Bragg value far away from the reflection conditions (upper part) for the two samples (a) and (b). On the left side the (AlAs)(GaAs)(004,0) SL satellite and on the right the GaAs(004) substrate reflection is visible. The angular scale is shown for both samples relative to the GaAs(004) Bragg angle $\theta_{(004)}$. For clarity, the photoelectron yield curves had been shifted down (a) and up (b) by 0.5 units.

The samples consisted of alternating epitaxial layers of AlAs and GaAs. They were grown by MBE on 0.6-nm thick GaAs(001) substrates. Both samples (a) and (b) described here had 460 AlAs/GaAs layer pairs and nearly equal layer thicknesses, but the growth temperatures were different. Sample (a) was grown at a substrate temperature of 610 °C and sample (b) at 660 °C. The intended layer thicknesses for each layer were 0.85 nm AlAs and 1.98 nm GaAs, corresponding to three double-atomic layers AlAs and seven double-atomic layers GaAs. To prevent chemical reactions of the AlAs with the ambient atmosphere, the short-period superlattice was finally capped with another 10 nm GaAs.

For an overview of the measurements, Fig. 1 shows the results of θ-scans for reflectivity R and photocurrent in the angular region around the (AlAs)(GaAs)(004,0) and the GaAs(004) substrate reflection. The incident angle θ is plotted relative to the GaAs(004) Bragg angle $\theta_{(004)} = 55.8553°$, which was determined by a fit of a theoretical rocking curve and was then used as a reference. Inspecting the logarithm of the reflectivity of both samples in the bottom part of the plot, different positions of the (AlAs)(GaAs)(004,0) main peak and different spacings between the thickness fringes are observable. These thickness

oscillations result from the interference of incident and reflected x-ray wave due to the change of the average index of refraction at the limiting interfaces of the SL structure.[15] The separation of the fringes in the reflectivity signal is a good measure for the total thickness of the SL stack, resulting in 1.36 μm (a) and 1.28 μm (b).

The SL 0th order peak corresponds to the average lattice-plane distances $\langle d^{\perp} \rangle$ in the SL's. The angle difference between the GaAs(004) and the 0th order SL peak can be used to calculate the relative concentration ratio of AlAs to GaAs. Preceding measurements on asymmetric reflections revealed already that the short-period SL forms a pseudomorphic lattice. The lattice plane distance of pseudomorphically grown AlAs between undistorted GaAs layers equals $d^{\perp}(\mathrm{AlAs}) = 0.14171\,\mathrm{nm}$. GaAs has a smaller value $d(\mathrm{GaAs}) = 0.141335\,\mathrm{nm}$. With these d values and using the center of the GaAs(004) and the (AlAs)(GaAs)(004,0) SL peak as the diffraction angle, the result for the relative lattice mismatch of the short-period SL is $\langle \Delta d/d^{\perp} \rangle = [\langle d^{\perp} \rangle - d(\mathrm{GaAs})]/d(\mathrm{GaAs}) = 8.17 \times 10^{-4}$ for sample (a) and 8.83×10^{-4} for sample (b). The corresponding average AlAs content is 31.3% (a) and 33.8% (b), which are both in reasonable agreement with the attempted 3:7 ratio. Nevertheless, the loss of Ga at the higher growth temperature can be expected, because of segregation effects.

In the upper part of Fig. 1, the simultaneously measured photoelectron yield I_e exhibits a completely different behavior than the reflectivity. This signal is strongly modulated by the standing wavefield inside the crystal. At the (AlAs)(GaAs)(004,0) satellite, modulations are observed that are typical for an XSW yield from atoms close to the diffraction planes, whereas at the GaAs(004) reflection, two maxima with a sharp dip in the middle of the rocking curve occur. Fringes due to the overall thickness are superposed, which are centered around the superlattice main peak and show a characteristic phase reversion at this angle. On the higher angle side, they are in phase with the reflectivity signal and on the lower angle side phase inverted. A comparison of the electron yield from sample (a) and (b) reveals further differences the modulation at (AlAs)(GaAs)(004,0) and in the relative intensity of the two peaks at GaAs(004), which are discussed in detail in Secs. III A and III B.

B. Principles

For an explanation of the observed features in the photoelectron and fluorescence yields, calculations based on the Takagi-Taupin differential equation have been carried out. In its general form, the Takagi-Taupin equations describe the x-ray diffraction from crystals with strain variations perpendicular to the surface.[11] The amplitude ratio $X = D_H/D_0$ depends on the phase shift between the complex amplitudes of incident and diffracted x-ray wave D_0 and D_H. Using X, the Takagi-Taupin equation can be written in the simple form[16]

$$-i\,dX/dT = X^2 - 2\eta X + 1, \tag{1}$$

with the deviation parameter η known from the dynamical theory of x-ray diffraction[17] and the reduced thickness T involving the structure factor of the reflection. This approach was originally developed to determine the reflectivity of heterostructures and superlattices,[16,18] but was extended in this paper to calculate the depth-dependent intensity of the wavefield $|D_0 + D_H|^2$ resulting from interference of incident and diffracted x-ray wave. Only σ polarization was taken into account, because of the experimental geometry and the linear polarization of synchrotron radiation. The recursion algorithm from Ref. 16 gives a dynamical description of the two-beam case, including substrate and superlattice reflection as well as thickness fringes. Note that the extinction of the incoming wave was calculated first in order to get the correct result for the wavefield intensity close to the substrate/SL interface. Another theoretical approach[19] takes this effect inherently into account.

After the complex amplitude ratio X and the local wavefield intensity $|D_0 + XD_0|^2$ has been computed as a function of incidence angle θ and position $p = \mathbf{H}\cdot\mathbf{r}$ at coordinates $\mathbf{r}$ in the lattice, the inelastic signal from each atom plane is calculated. The fluorescence signal probes a depth that depends on the absorption of the fluorescence photons and the take-off angle α. The take-off angle was set to 5° to reduce the contribution of Ga L and As L fluorescence from the substrate by a factor $> 5 \times 10^3$. Secondary core-hole excitations resulting from fluorescence radiation created in the sample are negligible. For all possible channels, a maximum influence of 1.3% was found for As fluorescence photons exciting electrons in the Ga L shell. The information depth of the Ga L fluorescence in the short-period SL is $\Lambda_{\gamma}(\mathrm{Ga\,L}\alpha) = 160\,\mathrm{nm}$, which means that surface defects and the GaAs cap are a small part of the total signal. The total fluorescence of each line can be calculated by a depth integration in which the contribution of an atomic plane in depth z is weighted by $\exp(-z/\Lambda_{\gamma})$.

In general, by comparing and fitting the normalized inelastic yield (XRF or electron) of the selected atomic species with the calculated yield, it is possible to determine the **H** Fourier component

$$A_H = |A_H|\exp(2\pi i\mathbf{H}\cdot\mathbf{r}) = \int_{\mathrm{u.c.}} a(\mathbf{r})\exp(2\pi i\mathbf{H}\cdot\mathbf{r})\,dV \tag{2}$$

of the corresponding atomic distribution function $a(\mathbf{r})$, with u.c. denoting the unit cell of the SL structure. This Fourier component is usually given by two real numbers between 0 and 1, the coherent fraction f_c and the position p, which are

$$f_c = |A_H| \quad \text{and} \quad p = \mathbf{H}\cdot\mathbf{r}. \tag{3}$$

If $p = 1.0$ the atomic positions are on the diffraction planes, and if $p = 0.5$ their position is exactly in between them. In such a one-position model, the coherent fraction f_c is equal to the fraction of atoms located at p divided by their Debye-Waller factor $\exp(-M)$ to correct for the thermal vibration amplitude. Two assumptions had to be made in order to restrict the computation time of such a fitting procedure for the short-period SL to a reasonable limit:

(i) The plane wavefield in the SL structure is periodic with $2\pi/|\mathbf{H}|$ in the direction of **H**, i.e., neither the changing electron density in the Al, Ga, and As layer, nor their slightly shifted position $p \neq 1.0$ resulting from the data evaluation, changes the XSW field calculated from the original heteroepitaxial atomic positions.

(ii) The depth dependence of the wavefield can be neglected, because of the small information depths Λ of the fluorescence and electron signals, i.e., the same XSW field distribution in each bilayer with period d_{SL} was used as it was calculated for the uppermost bilayer of the SL. Therefore, the normalized intensity of the XSW field is $|1+X|^2$.

An angular offset $\Delta\theta$ and a scaling factor for the reflectivity was determined by a fit of the calculated reflectivity curve to the measured reflected intensity. Using $\Delta\theta$, the normalized intensity of the XSW field $I(\theta,p,f_c)$ was calculated in two steps: First, a database was created, in which the calculated XSW field intensity $I_c(\theta,p_n)$ was stored for each measurement point in steps of $\Delta p=0.0025$, for $0\leqslant p_n\leqslant 1$, i.e., one wavefield period length. This stepwidth Δp is sufficiently small with respect to the confidence intervals of the fit results. For the (AlAs)(GaAs)(004,0) SL satellite, the wavefield period length is $\langle d^{\perp}\rangle$, and for the GaAs(004) substrate reflection, it is $d_{(004)}$. The normalized intensity can then be calculated from $I(\theta,p,f_c)=f_cI_c(\theta,p)+\Delta p(1-f_c)\Sigma_nI_c(\theta,p_n)$. By this, the time-consuming calculation of the XSW field in the SL structure was done only once and not for every iteration during the fit.

In principle, the normalized atomic-distribution function $a(\mathbf{r})$ could be synthesized, if enough reflections, i.e., A_H, were measured:

$$a(\mathbf{r})=\Sigma_H A_H\exp(-2\pi i\mathbf{H}\cdot\mathbf{r})=a_0+\Sigma_{j=1}^{J}a_j\delta(\mathbf{r}-\mathbf{r}_j). \tag{4}$$

Since the sample can be viewed as a layered structure normal to the surface, in our evaluation, model assumptions for the atomic distribution in the **H** direction had to be made. In Eq. (4), a_0 represents the fraction of randomly located atoms, and a_j the fraction of J atoms located at coordinates $\mathbf{r}_j$, with $a_0+\Sigma_{j=1}^{J}a_j=1$ and δ denoting the delta function. Each J-position model results in a number for the atomic position

$$p=(2\pi)^{-1}\times\arctan[\Sigma_{j=1}^{J}a_j\sin(2\pi\mathbf{H}\cdot\mathbf{r}_j)/\Sigma_{j=1}^{J}a_j\cos(2\pi\mathbf{H}\cdot\mathbf{r}_j)], \tag{5}$$

and the coherent fraction

$$f_c=\{[J^{-1}\Sigma_{j=1}^{J}a_j\sin(2\pi\mathbf{H}\cdot\mathbf{r}_j)]^2+[J^{-1}\Sigma_{j=1}^{J}a_j\cos(2\pi\mathbf{H}\cdot\mathbf{r}_j)]^2\}^{1/2}, \tag{6}$$

which can be used to adapt the model until the result is in best agreement with the measurement.

The model of the short-period SL samples (a) and (b) employed for the computation consisted of 460 $(\mathrm{AlAs})_3(\mathrm{GaAs})_7$ layer pairs on the GaAs(001) substrate [see Fig. 2(a)] capped by a 10 nm GaAs layer. For the AlAs layers, perfect pseudomorphic growth between the relaxed GaAs parts was supposed, resulting in a tetragonal distortion of the cubic AlAs unit cell by $\Delta a/a=1.362\times10^{-3}$. Accordingly, in the model, the thicknesses of the AlAs and GaAs layers were 0.85026 nm and 1.97869 nm. Results for the off-Bragg normalized intensity of the standing wave on the atomic planes, depending on incident angle θ and depth z in the SL structure, are presented in Fig. 3.

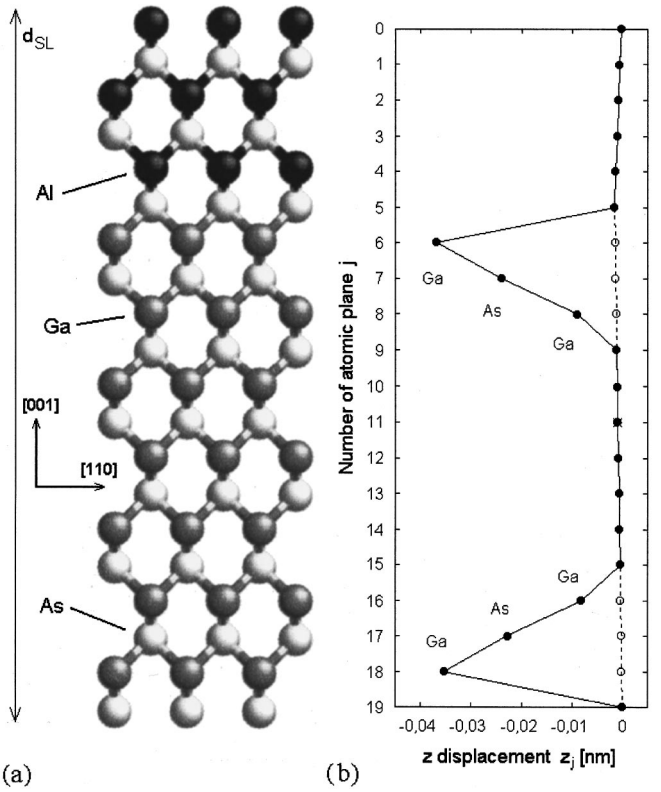

FIG. 2. (a) Model of one unit cell of an $(\mathrm{AlAs})_3(\mathrm{GaAs})_7$ short-period superlattice. The SL period length for perfect pseudomorphic growth is $d_{\mathrm{SL}}=2.82895$ nm. The samples consisted of 460 periods grown on a GaAs(001) substrate along the [001] direction. (b) Calculated displacements z_j along the [001] direction according to the model, which is discussed in Sec. III A. The position z_j is given relative to planes defined by the average lattice-plane distances $\langle d^{\perp}\rangle$. Open circles represent the situation without displacements.

At the angular position of the 0th order SL satellite, this field distribution can be interpreted assuming that the periodicity of the wavefield is equal to the average (004) lattice plane distance $\langle d^{\perp}\rangle$ in the AlAs/GaAs stack. Therefore, the total number of diffraction planes in the short-period SL, or nodes and antinodes of the wavefield, is equal to the number of contributing atomic planes. In case of the superlattice (004, 0) reflection, these atomic planes consist of alternating monolayers of Ga and As, or Al and As, as shown in Fig. 2(a). They have an almost equal separation from each other, because the difference between $d^{\perp}(\mathrm{AlAs})$ and $d^{\perp}(\mathrm{GaAs})$ is only 0.000375 nm. The average atomic position is located on the diffraction planes, i.e., $p=1$. Near the surface at $z=0$, at the (AlAs)(GaAs)(004,0) satellite, the calculated wavefield in Fig. 3 in its overall shape resembles the observed angular dependence of the photoelectron yield shown in Fig. 1. As will be shown later, this can be explained by the small information depth Λ_e of the photocurrent signal. Decreasing contrast of the modulation and a dip in the local intensity of the wavefield can be observed at large depths, because of the dynamical extinction effect and the redirection of energy flow into the diffracted beam. The separation between the maxima of the thickness fringes is increasing with depth, but the SL satellite remains in the center of these structures. Note that the fringe pattern is pinned to the angular position of the

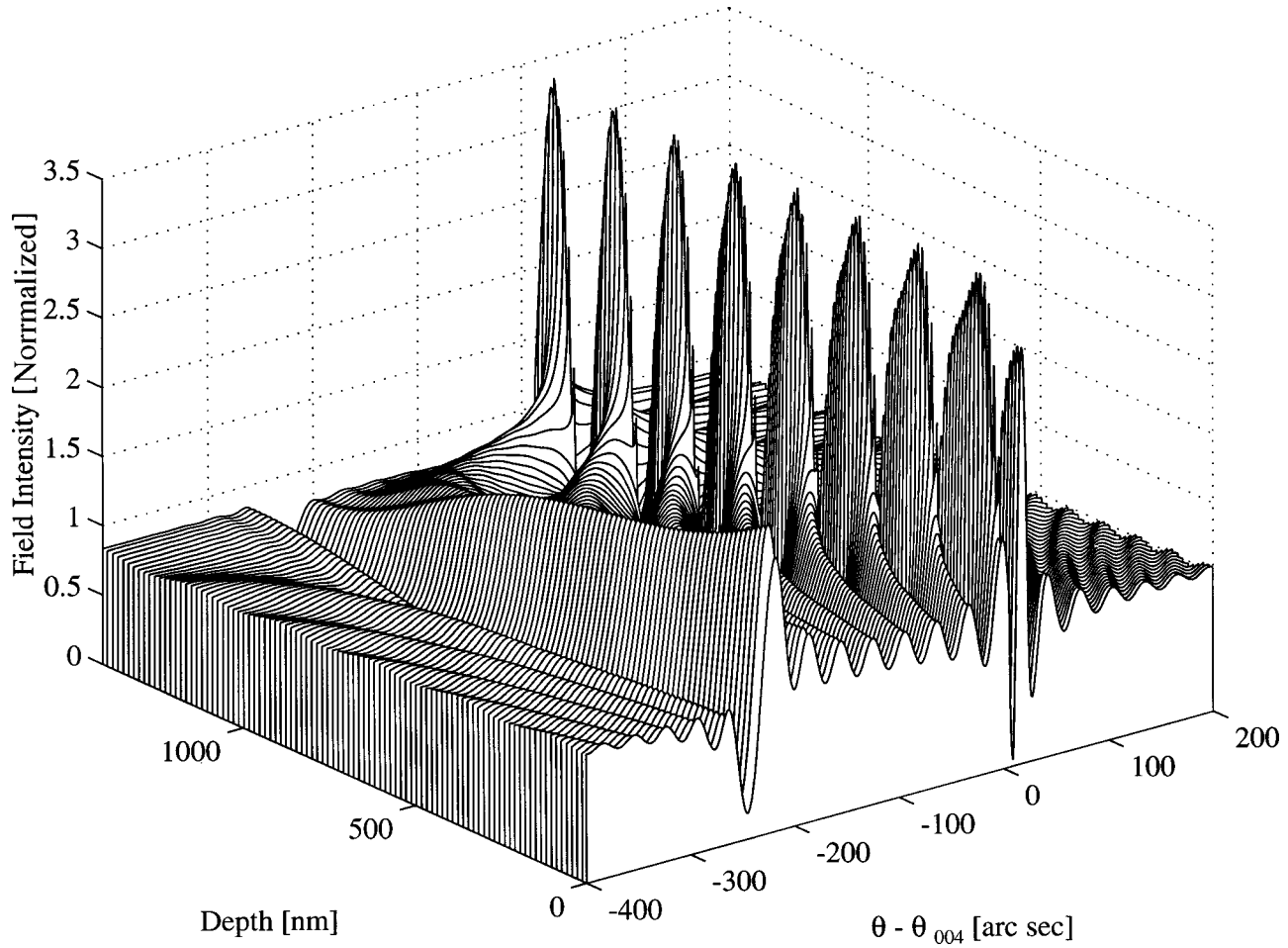

FIG. 3. Calculation of the intensity of the wavefield on the atomic planes in the superlattice in dependence of incidence angle and depth z in the AlAs/GaAs SL stack. The normalized intensity is given at the regular atom planes of the short-period SL ($p=0$) spaced by $\langle d^{\perp}\rangle$. The modulation at -300 arc sec$<\theta-\theta_{(004)}<200$ arc sec is due to the (AlAs)(GaAs)(004,0) SL satellite, whereas the structure around $\theta-\theta_{(004)}=0$ arc secis resulting from a moiré effect of the GaAs(004) substrate wavefield. The GaAs substrate extends beyond $z\approx 1300$ nm and is not shown in the plot.

satellite reflection and shows the experimentally observed phase reversion with respect to the reflectivity.[20]

A different picture appears at the GaAs(004) substrate reflection. In this case, the depth dependence of the yield is characterized by several maxima, which exhibit a decreasing modulation ascending from the substrate-superlattice interface to the surface. These maxima arise from the GaAs(004) substrate wavefield extending into the AlAs/GaAs SL region. For $(AlAs)_3(GaAs)_7$, the relative difference of 7.96×10^{-4} between the substrate wavefield periodicity and the average diffraction plane spacing $\langle d^{\perp}\rangle$ of the short-period SL results in a beating or moiré effect with maximum photoexcitation if the antinodes of the wavefield coincide with the Ga, Al, and As planes. This situation occurs about eight times over the whole thickness T of the SL ($T/\Lambda_M=1360/173.1=7.86$, where Λ_M is the repetition length of the moiré pattern (see Sec. III B). Between these maxima, the atomic planes are located at virtually any position $0\leqslant p\leqslant 1$ with respect to the wavefield. The regular pattern from the thickness fringes is superposed, which results in more complicated modulations during a scan of the rocking curve. Depending on the actual thickness of the SL structure, the moiré pattern is truncated at a certain distance from the substrate-superlattice interface at the upper side of the sample. Thus, the resulting XSW-induced modulation of a signal like the electron yield, which is probing only a thin surface layer, is strongly influenced by the actual SL thickness, the period length of the moiré pattern and the information depth of the secondary reaction channel.

III. RESULTS AND DISCUSSION

A. (AlAs)(GaAs)(004,0) superlattice satellite

In order to use an element-specific XSW yield signal, fluorescence radiation from the sample was monitored by a solid state x-ray detector. Figure 4 shows the region of interest of a fluorescence spectrum from the sample, recorded at an angular position far away from Bragg reflections. The intensities of the Ga L, As L, and Al K fluorescence emission were separated by a deconvolution using three Gaussian functions to include a detector resolution of 150 eV full width at half maximum. The results for the off-Bragg normalized intensity—meaning the intensity normalized to a θ region where no Bragg diffraction is excited—of the three fluorescence lines from sample (a) as well as the photocurrent yield from sample (a) and (b) are plotted versus θ (Fig. 5). The solid lines are best fits from least-squares minimiza-

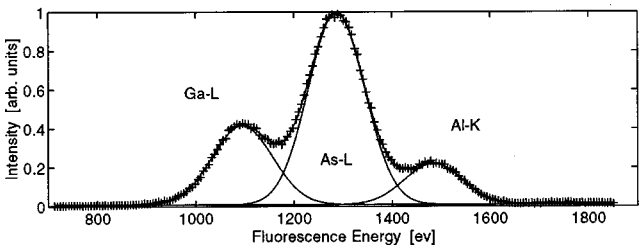

FIG. 4. X-ray fluorescence spectrum measured with the thin-window solid state Si(Li) detector. For an accurate intensity determination of the Ga L, As L, and Al K fluorescence, three Gaussian profiles were fitted to the spectrum at each angular position θ.

tions of calculated modulations. In case of the electron yields, the fits were not performed with depth integrated wavefield intensities, because of the small information depth Λ_e of this signal. Instead, the result for the wavefield at the surface was directly used. The fit parameters under variation are the position p and the coherent fraction f_c of atoms. Derived results for p and f_c are summarized in Table I. Furthermore, it is worth mentioning that the calculated width of the (AlAs)(GaAs)(004,0) satellite, the intensity ratio to the GaAs(004) substrate reflection, and the thickness fringes are in good agreement with the experiment, revealing that angular and energy resolution were sufficient and sample curvature[21] was beneath notice.

Evaluating only the photoelectron yield, the result for p of both samples indicates identical atomic positions. Within the statistical error of $\pm 1\%$, the coherently ordered atoms are located on the diffraction planes. Of special interest is the coherent fraction, which shows a large difference of 8% between samples (a) and (b). An explanation for this sample-dependent result can be found in the different epitaxial quality in a region equivalent to the electron information depth Λ_e, which is about 64 nm (see Sec. III B). Sample (b) was prepared at the higher substrate temperature of 660 °C. It yields a larger coherent fraction f_c and has, therefore, less defects and a more perfect crystallinity. This can be attributed to enhanced surface mobility and a more efficient dissociation of the adsorbed molecules during epitaxial growth. Another reason for the difference may be a reduced crystal perfection in the surface region due to chemical reactions with the ambient atmosphere or with impurities. The influence of this effect can be estimated from the ratio of the thickness of the distorted layer[23] and the average thickness contributing to the electron signal, which is about 2%. Since the surface reactions are expected to be comparable for both samples, the resulting f_c values of the electron yield are a good measure of the epitaxial perfection in the short-period SL and not in the surface region. Note that measurements on the (AlAs)(GaAs)(004±1) satellites, showed intensive satellite reflections with x-ray diffraction but did not exhibit XSW-induced modulations.

For an element specific investigation, the XSW fluorescence yields were measured from sample (a). The fluorescence XSW yield probes a depth that is characterized by the information depth, e.g., $\Lambda_\gamma(\mathrm{Ga\,L}\alpha) = 160$ nm for the Ga L fluorescence in our short-period SL's. This means that surface defects and the GaAs cap are a small part of the total signal. Note also that the fluorescence information depth is roughly twice that of the electron information depth. In order

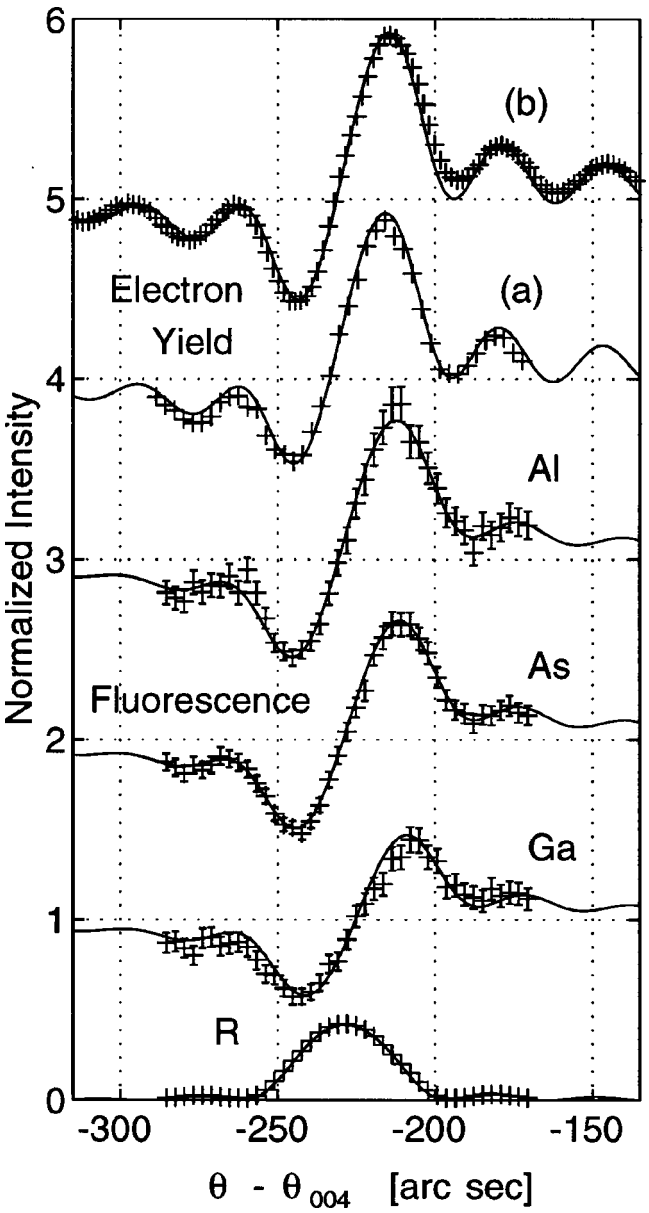

FIG. 5. Reflectivity R, modulation of the Al K, As L, and Ga L fluorescence yield from sample (a), and photocurrent yield for both samples (a) and (b), at the 0th order SL satellite (AlAs)(GaAs)(004,0). For the upper four curves, offsets of 1, 2, 3, and 4 had been added and, in addition, the photocurrent from sample (b) was shifted to 20 arc sec larger θ to match the angular scale of sample (a). Solid lines correspond to least-squares fitted theoretical calculations resulting in the parameters presented in Table I.

to calculate the total fluorescence collected by the detector, a depth integration was performed and the contribution of an atomic plane in depth z was weighted by $\exp(-z/\Lambda_\gamma)$.

The results for Al K, As L, and Ga L fluorescence summarized in Table I exhibit not only different coherent fractions f_c for the different elements, but also a significant difference in their positions p relative to the diffraction planes. In the case of the Al atoms, which represent the AlAs parts of the short-period SL, the largest coherent fraction $f_c(\mathrm{meas})(\mathrm{Al}) = 0.95$ and an average position on the diffraction planes is found. Such a high-coherent fraction indicates a nearly perfect epitaxial quality of these layers and its dif-

TABLE I. p and f_c(meas) of samples (a) and (b) resulting from least-squares fits to the (AlAs)(GaAs)(004,0) SL peak data from fluorescence and photoelectron yield measurements depicted in Fig. 5. The confidence intervals are estimated from the statistical error in the experimental data. The measured XRF data f_c(meas) are divided by the Debye-Waller-factor (DWF) $\exp(-M)$ (Ref. 22) to obtain the corrected f_c.

	Al (a)	As (a)	Ga (a)	I_e (a)	I_e (b)
p	0.99 ± 0.02	0.97 ± 0.01	0.92 ± 0.02	1.00 ± 0.01	0.99 ± 0.01
f_c(meas)	0.95 ± 0.03	0.86 ± 0.02	0.73 ± 0.03	0.74 ± 0.02	0.82 ± 0.01
DWF	0.95	0.93	0.92		
f_c	1.00 ± 0.03	0.92 ± 0.02	0.79 ± 0.03		

ference from unity is due to the thermal vibrations. On the other hand, the Ga L fluorescence exhibits a lower coherent fraction and also $p(\mathrm{Ga})=0.92\pm0.01$ shows a significant deviation from Ga positions $p(\mathrm{Ga})=1.0$ on the diffraction planes. The values for As are between those for Al and Ga, since As is part of both AlAs and GaAs layers and gives average information. In the evaluation, we took into account the following Debye-Waller factors: $\exp(-M)=0.95\,(\mathrm{Al})$, $\exp(-M)=0.92\,(\mathrm{Ga})$, and $\exp(-M)=0.93\,(\mathrm{As})$. These Debye-Waller factors are based on data for bulk AlAs and GaAs.[22] Assuming isotropic thermal vibrations, the coherent fraction resulting from the measurement f_c(meas) has been corrected due to $f_c=f_c(\mathrm{meas})/\exp(-M)$.

By the measurement of the XSW yields at the (AlAs)(GaAs)(004,0) reflection, we could determine p and f_c for Al, Ga, and As, that means all together six parameters. In the superlattice unit cell of our model there are three Al, seven Ga, and ten As atom planes. Therefore, in the general case, 20 $\mathbf{r_j}$ coordinates have to be determined. Using the six equations [Eqs. (5) and (6)] for Al, Ga, and As, strictly speaking, a unique solution cannot be given. However, (i) if we do not differentiate between equivalent atom arrangements, (ii) if we look for arrangements with deviations as small as possible, and (iii) if we assume that displacements are more likely at the interfaces, then we can give an atom model.

The significant deviations of $f_c(\mathrm{Ga})=0.79\pm0.02$ and $f_c(\mathrm{As})=0.92\pm0.02$ from unity can only be explained if the preferred occupation of more than one Ga or As position relative to the diffraction planes is considered. Since $p(\mathrm{Ga})=0.92\pm0.02$ and $p(\mathrm{As})=0.97\pm0.01$ are between 0.5 and 1.0, it can be concluded straightforward that in each SL unit cell there must be a net displacement of the Ga and the As atom planes along the [001] direction. This noninversion symmetric displacement within the SL unit cell might be explained by a preferential strain given by the growth direction. The net z displacement towards the substrate is in contradiction to the findings of Harada and co-workers[4] on their SL's, which suggest a model with symmetric displacements of equivalent atom fractions along the [001] and [001] direction, which preserve an inversion symmetry in the middle of each layer.

In the quantitative analysis, using Eqs. (6) and (7), p and f_c of different models are calculated and compared with the experimental p and f_c values for Al, As, and Ga. The best agreement is achieved with an $(AlAs)_3(GaAs)_7$ unit cell in which four Ga atom planes and two As atom planes are shifted from the (004,0) diffraction planes, i.e., 4/7 of the Ga atoms and 2/10 of the As atoms. Within a statistical error of $\pm5\%$, the resulting displacements compatible with the experimental values for p and f_c are $z_j=-0.250\langle d^{\perp}\rangle=-0.035\,\mathrm{nm}$ for the outermost Ga atom planes, $z_j=-0.055\langle d^{\perp}\rangle=-0.0078\,\mathrm{nm}$ for the two next Ga atom planes, and $z_j=-0.160\langle d^{\perp}\rangle=-0.023\,\mathrm{nm}$ for the two outermost As atom planes in the GaAs layer of the unit cell. All the other Ga and As atom planes, as well as the Al atom planes are at the ideal diffraction planes $z_j=0$, besides the negligible deviations within the unit cell due to the differences between $d^{\perp}(\mathrm{AlAs})=0.14\,1710\,\mathrm{nm}$ and $d^{\perp}(\mathrm{GaAs})=0.14\,1335\,\mathrm{nm}$. The resulting structural model of the $(AlAs)_3(GaAs)_7$ unit cell is presented in Fig. 2(b). A possible shift of the atomic planes at the interfaces has also been pointed out theoretically by Min, Massidda, and Freeman.[24] However, the bond length variations resulting from our model are larger than usually observed or theoretically predicted. With XSW on the (004,0) reflection only, we cannot decide which of the ten As atom planes and which of the seven Ga atom planes of the SL unit cell are displaced. However, from growth kinetics, it is more likely that the displacements occur at the interfaces rather than in the bulk. Assuming that only the atomic planes in the GaAs layers closest to the interfaces to the AlAs are affected, compared to other models, the displacements along the [001] direction are rather small.

B. GaAs(004) substrate reflection

In contrast to the (AlAs)(GaAs)(004,0) wavefield, the GaAs(004) substrate wavefield has a slightly different period length compared to the periodicity of the atomic planes in the short-period SL. This results in a moiré pattern as shown in Fig. 3. The atomic layers in different depths in the SL are located at virtually all atomic positions p relative to the wavefield periodicity given by the substrate lattice. Averaging over all XSW phase contributions can only be avoided if the depth from where the signal is collected is limited to a small region of the moiré pattern. Therefore, the XSW induced modulation strongly depends on the information depth of the signal under inspection.

The information depth Λ_e of the electron yield is limited by the mean-free-path of the electrons and the resulting photoelectron current originates from a rather small depth. In the measurement presented in Fig. 6, this effect results in pronounced structures in the electron yield, whereas the fluorescence yields roughly resemble the rocking curve. An analysis of the observed fluorescence yields by least-squares fits of

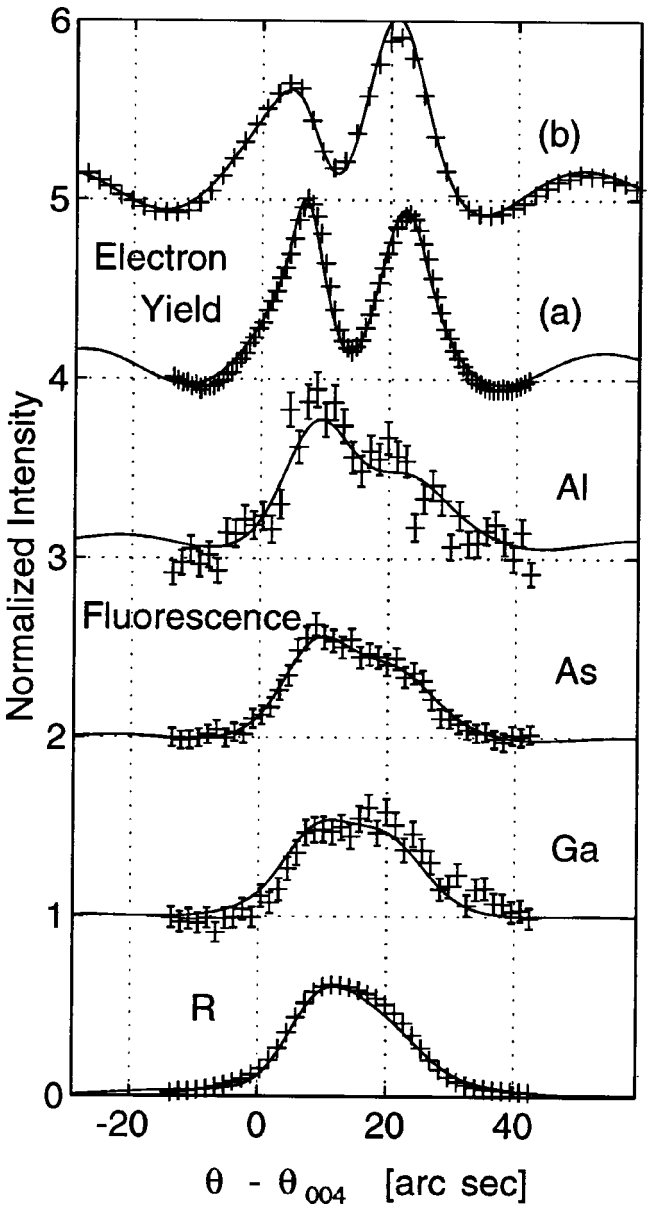

FIG. 6. Photoelectron yield for samples (a) and (b), as well as Al, As, and Ga fluorescence from sample (a), obtained from an XSW measurement at the GaAs(004) substrate reflection. For reasons of clarity, 1, 2, 3, and 4 units had been added to the upper four curves. Symbols indicate data points. The solid lines are least-squares fits of the theory described in the text. Fit results are summarized in Table II. The GaAs(004) substrate rocking curve *R* appears at the bottom.

calculated curves reveals an incoherent atomic distribution with respect to the wavefield periodicity. The results for p and f_c are summarized in Table II.

The GaAs(004) rocking curve has the same width as theoretically predicted, indicating very good experimental resolution and no observable dispersion. In case of the electron signal, an additional Gaussian convolution with 10 arcsec (FWHM) was performed and clearly improved the fit. Since the structural quality of the SL used is very close to ideal, this required smearing of the yield signal is due to the limited spatial coherence of the x-ray wavefield, which extends from the substrate over the 1.36 μm (a) and 1.28 μm (b) thick SL structure up to the surface. From the monochromatization $\Delta\lambda$ and collimation $\Delta\theta$ of the incident beam with wavelength λ, a longitudinal coherence length $\lambda^2/2\Delta\lambda \approx 2$ μm and a transverse coherence length $\lambda/\Delta\theta \approx 7.4$ μm can be deduced,[25] and a loss of phase contrast near the surface can be expected, since the maximum pathlength difference of beams across the full SL is up to 1.6 μm. A detailed analysis of this coherence effect is not attempted here since it requires a further modification of the dynamical theory. Note that the mutual interaction between the wavefields from the (AlAs-)(GaAs)(004,0) satellite and the substrate reflection[26] is included in this calculation.

As a consequence of the low-coherent fractions f_c in case of the three fluorescence yields, reliable phase information from the GaAs(004) reflection cannot be extracted. The low f_c values are a result of the information depth Λ_γ and are not due to the sample quality. Because of the known depth dependency of the interference field structure inside the SL, the electron yield allows a rather detailed analysis of its information depth Λ_e in turn. Nevertheless, the electron yield allows a more precise analysis of its information depth Λ_e than reached by other methods.[10] The position p and the coherent fraction f_c of this signal are interpreted as phase and amplitude of the Fourier components of the weighted atomic-distribution function $A_{(004)}(\mathrm{Al})$, $A_{(004)}(\mathrm{Ga})$, and $A_{(004)}(\mathrm{As})$. The weighting is included by the factor $\exp(-z/\Lambda_e)$ so that the contribution to the position p_n of atom layer n depends on the depth $z_n = n\langle d^\perp\rangle$. It is assumed that the moiré pattern has a repetition length Λ_M given by $\Lambda_M = \langle d^\perp\rangle d(\mathrm{GaAs})/(\langle d^\perp\rangle - d(\mathrm{GaAs}) = 173.1\,\mathrm{nm}$ (a) and 160.2 nm (b). Sample (a) has a smaller AlAs content, thus resulting in an average lattice-plane distance $\langle d^\perp\rangle$ closer to that of the GaAs(004) wavefield periodicity and, consequently, in a longer repetition length Λ_M. The parameters that are varied to bring the XSW results from Table II in

TABLE II. p and f_c(meas) of samples (a) and (b) resulting from least-squares fits to the (AlAs)(GaAs)(004) substrate peak data from fluorescence and photoelectron yield measurements shown in Fig. 6. The confidence intervals are estimated from the statistical error in the experimental data. The measured XRF data f_c(meas) are divided by the (DWF) $\exp(-M)$ (Ref. 22) to obtain the corrected f_c.

	Al (a)	As (a)	Ga (a)	I_e (a)	I_e (b)
p	0.34 ± 0.24	0.42 ± 0.31	0.55 ± 0.39	0.49 ± 0.03	0.59 ± 0.03
f_c(meas)	0.16 ± 0.07	0.09 ± 0.03	0.07 ± 0.04	0.39 ± 0.03	0.35 ± 0.02
DWF	0.95	0.93	0.92		
f_c	0.17 ± 0.07	0.10 ± 0.03	0.08 ± 0.04		

agreement with this model are the position p_0 of the uppermost atomic layer of the SL and Λ_e. A Debye-Waller factor of 0.95, resulting from $f_c(\mathrm{Al})=0.95$ in Table I, is included for thermal vibrations and static disorder.

For both samples, comparable information depths of $\Lambda_e = (62\pm5)$ nm (a) and (65 ± 3) nm (b)have been found. As these results are mainly determined by the coherent fraction f_c, the small difference can be attributed to the GaAs cap, which has not yet been considered. Although its nominal thickness of 10 nm is thin compared to Λ_e, disorder in the surface region may result in a slight decrease of f_c. Taking into account that the electron yield was measured as a total photocurrent I_e,[14] the result for Λ_e can be explained by the large mean-free-path of the scattered low-energetic electrons. The derived positions of the uppermost atomic planes of the short-period SL structure are $p_0=0.67\pm0.04$ (a) and 0.77 ±0.04 (b) (0 in p_0 indicates the uppermost atomic plane). These results differ from p in Table II because of the depth integration. If, for example, the position of one Al layer coincides with $p=1$ of the GaAs(004) wavefield, an Al layer at a greater depth is located at $p<1$, because $\langle d^{\perp}\rangle$ is larger than $d_{(004)}$. This means that the positions p of the AlAs atomic planes decrease with increasing depth, until one moiré repetition length Λ_M is reached. Using this periodicity, the expected values for p_0 would be 0.54 (a) and 0.12 (b), which are different from the actual results given above. Due to the identical lattice parameters in the substrate and in the GaAs cap, an additional shift of p_0 cannot result from the cap, because the periodicity of the GaAs(004) wavefield is the same as the lattice-plane distance in the cap.

For an interpretation, however, it has to be considered that the absolute accuracy of these measurements is of the order 0.005 nm with respect to the total thickness of the SL structures. Deviations due to a contraction at the interfaces between the AlAs and GaAs parts can easily add up over the 460 layer pairs, resulting in a slightly different repetition length Λ_M of the moiré pattern. Such displacements of Ga and As atoms from their ideal lattice positions have already been encountered in the measurements at the (AlAs)(GaAs)(004,0) superlattice satellite (Sec. III A). Note that the results for Λ_e are not affected by such displacements.

IV. CONCLUSION

XSW measurements, using fluorescence radiation and total electron yield as inelastic signals, were performed on $(AlAs)_m(GaAs)_n$ short-period SL. The results are in good agreement with dynamical calculations for the depth- and angle-dependent wavefield based on the Takagi-Taupin theory. Around the (AlAs)(GaAs)(004,0) satellite, the wavefield was used to study the atomic arrangement in the AlAs and GaAs layers. It turned out that the AlAs parts are nearly perfectly ordered with respect to the wavefield, whereas a fraction of the Ga and As atoms occupy additional, nonideal positions. The results are consistent with a model in which an internal relaxation of Ga and As atoms at the interfaces between the AlAs and GaAs layers occurs. A straightforward analysis of the data reveals that a part of the Ga and As atom planes are displaced towards the substrate, i.e., in [001] direction. By fitting the data, a model for the atomic distribution along the [001] direction can be determined. In this model, at each AlAs/GaAs interface, of the GaAs layers, two Ga atom planes are displaced by 0.035 and 0.008 nm and of the GaAs layers, one As atom plane is displaced by 0.023 nm. The displacements exhibit mirror symmetry within the GaAs layer.

The nonelement-specific total-electron yield appears to be a good measure of the crystallinity in the surface region, thus offering an additional method for characterization of superlattices. From the measurements of the total electron yield at the GaAs(004) reflection the information depth Λ_e of this signal was determined. Due to the small information depth of the electron signal, only a thin surface layer is probed, where the difference between wavefield periodicity $d_{(004)}$ and $\langle d^{\perp}\rangle$ does not result in an averaging over all atomic positions. An information depth of the total-electron yield of 64 nm was deduced from the data.

ACKNOWLEDGMENTS

SSRL was funded by the Department of Energy, Office of Basic Energy Sciences, under Contract No. DE-AC03-76SF00515. Two of us, M.S. and G.M., are grateful to the Volkswagen Stiftung for sponsoring their studies through a grant to Stanford University. G.M. also acknowledges valuable discussions with F. Chuckhovskii, D. Novikov, and S. Stephanov.

*Present address: Rich. Seifert & Co., Röntgenwerk, Branch office Munich, Mannertstr. 36, D-80997 Munich, Germany.

†Present address: Argonne National Laboratory, Material Science Division, Argonne, IL 60439.

[1] A. Segmüller and A. E. Blakeslee, J. Appl. Crystallogr. **6**, 19 (1973); A. Segmüller, P. Krishna, and L. Esaki, *ibid.* **10**, 1 (1977); J. Kervarec, M. Baudet, J. Caulet, P. Auvray, J. Y. Emery, and A. Regreny, *ibid.* **17**, 196 (1984); V. S. Speriosu and T. Vreeland, J. Appl. Phys. **56**, 1591 (1984).

[2] R. M. Fleming, D. B. McWhan, A. C. Gossard, W. Wiegmann, and R. A. Logan, J. Appl. Phys. **51**, 357 (1980); P. F. Fewster, J. Appl. Crystallogr. **21**, 524 (1988).

[3] M. Schuster, A. Lessmann, A. Munkholm, S. Brennan, G. Materlik, and H. Riechert, J. Phys. D **28**, A206 (1995).

[4] J. Harada, Y. Kashihara, M. Sakata, M. Mashita, and Y. Ashizawa, Jpn. J. Appl. Phys., Part 2 **24**, L62 (1985); Y. Kashihara, T. Kase, and J. Harada, *ibid.* **25**, 1834 (1986); Y. Kashihara and J. Harada, *ibid.* **27**, 522 (1988).

[5] P. L. Cowan, J. A. Golovchenko, and M. F. Robbins, Phys. Rev. Lett. **44**, 1680 (1980); N. Hertel, G. Materlik, and J. Zegenhagen, Z. Phys. B **58**, 199 (1985); T. Ohta, H. Sekiyama, Y. Kitajima, H. Kuroda, T. Takahashi, and S. Kikuta, Jpn. J. Appl. Phys., Part 2 **24**, L475 (1985); E. Vlieg, A. E. Fischer, J. F. van der Veen, B. N. Dev, and G. Materlik, Phys. Rev. B **36**, 4769 (1987).

[6] For reviews, see J. Zegenhagen, G. Materlik, and W. Uelhoff, J. X-ray Sci. Technol. **2**, 214 (1990); J. Zegenhagen, Surf. Sci. Rep. **18**, 199 (1993).

[7] A. Iida, T. Matsushita, and T. Ishikawa, Jpn. J. Appl. Phys., Part 2 **24**, L675 (1985); S. I. Zheludeva, M. V. Kovalchuk, N. N.

Novikova, I. V. Bashelhanov, N. Salaschenko, A. D. Akhsakhalyan, and Y. Y. Platonov, Rev. Sci. Instrum. **63**, 1 (1992); T. Kawamura and H. Takenaka, J. Appl. Phys. **75**, 3806 (1994).

[8] M. J. Bedzyk, G. M. Bommarito, and J. S. Schildkraut, Phys. Rev. Lett. **62**, 1376 (1989).

[9] For the sake of simplification, in the following text we omit the index H in $f_{c,H}$ and p_H.

[10] M. J. Bedzyk, G. Materlik, and M. V. Kovalchuk, Phys. Rev. B **30**, 4881 (1985); M. V. Kovalchuk, D. Liljequist, and V. G. Kohn, Fiz. Tverd. Tela (Leningrad) **28**, 3409 (1986) [Sov. Phys. Solid State **28**, 1918 (1986)].

[11] S. Takagi, Acta Crystallogr. **15**, 1311 (1962); D. Taupin, Bull. Soc. Fr. Mineral. Cristallogr. **87**, 469 (1964); S. Takagi, J. Phys. Soc. Jpn. **26**, 1239 (1969).

[12] N. J. Shevchik and D. A. Fischer, Rev. Sci. Instrum. **50**, 577 (1979).

[13] Quantum-window detector with an active area of 10 mm^2, Kevex Corporation, Foster City, California.

[14] A. Lessmann, M. Schuster, S. Brennan, G. Materlik, and H. Riechert, Rev. Sci. Instrum. **66**, 1428 (1995).

[15] P. Croce, G. Devant, M. Gandais, and A. Marraud, Acta Crystallogr. **15**, 424 (1962); R. W. Vook, T. Parker, and D. Wright, in *Surfaces and Interfaces* (Syracuse University Press, Syracuse, NY, 1967), Vol. I, pp. 347–358.

[16] W. J. Bartels, J. Hornstra, and D. W. Lobeek, Acta Crystallogr., Sect. A: Found Crystallogr. **42**, 539 (1986).

[17] B. W. Batterman and H. Cole, Rev. Mod. Phys. **36**, 681 (1964).

[18] M. A. G. Halliwell, M. H. Lyons, and M. J. Hill, J. Cryst. Growth **68**, 523 (1984).

[19] S. A. Stepanov, E. A. Kondrashkina, R. Köhler, D. V. Novikov, G. Materlik, and S. M. Durbin, Phys. Rev. B **57**, 1 (1998).

[20] On the lower-angle side of the (004,0) satellite, the nodes, and on the higher-angle side, the antinodes, of the standing wavefield coincide with the atomic planes. Proceeding from lower to higher angle, the resulting phase shift of the standing wavefield equals π, with the antinodes shifting in $-\mathbf{H}$ direction from a position between to a position on the atomic planes. Compared to a situation without fringes, the XSW field intensity is now periodically increased on the lower-angle side and decreased on the higher-angle side due to the superposition of the field associated with the thickness fringes.

[21] A curvature radius of 107 m, corresponding to approximately 2 arc sec angular broadening, can be calculated from the theory of elasticity.

[22] *Numerical Data and Functional Relationships in Science and Technology*, edited by O. Madelung, Landolt Börnstein, New Series, Group III, Vol. 22, Pt. a (Springer, Berlin, 1987).

[23] R. W. Bernstein and J. K. Grepstad, Surf. Interface Anal. **14**, 109 (1989).

[24] B. I. Min, S. Massidda, and A. J. Freeman, Phys. Rev. B **38**, 1970 (1988).

[25] I. K. Robinson, R. Pindak, R. M. Fleming, S. B. Dierker, K. Ploog, G. Grübel, D. L. Abernathy, and J. Als-Nielsen, Phys. Rev. B **52**, 9917 (1995).

[26] A. Authier, J. Gronkowski, and C. Malgrange, Acta Crystallogr., Sect. A: Found. Crystallogr. **45**, 432 (1989).